Application of Machine Learning to Characterize Gas Hydrate Reservoirs in Mackenzie Delta (Canada) and on the Alaska North Slope (USA)

Leebyn Chong[1,2], Harpreet Singh[3,4], Christopher G. Creason[5,6],
Yongkoo Seol[3], Evgeniy M. Myshakin*[1,2]

[1]*National Energy Technology Laboratory, 626 Cochrans Mill Road, P.O. Box 10940, Pittsburgh, PA 15236, USA*
[2]*NETL Support Contractor, 626 Cochrans Mill Road, P.O. Box 10940, Pittsburgh, PA 15236, USA*
[3]*National Energy Technology Laboratory, 3610 Collins Ferry Road, Morgantown, WV 26507, USA*
[4]*NETL Support Contractor, 3610 Collins Ferry Road, Morgantown, WV 26507, USA*
[5]*National Energy Technology Laboratory, 1450 Queen Avenue SW, Albany, OR 97321, USA*
[6]*NETL Support Contractor, 1450 Queen Avenue SW, Albany, OR 97321, USA*

Abstract

The artificial neural network was utilized to train machine learning (ML) models to predict gas hydrate saturation distributions in permafrost-associated deposits in the Eileen Gas Hydrate Trend on the Alaska North Slope (ANS), USA and in the Beaufort-Mackenzie Basin, Northwest Territories, Canada. The database of Logging-While-Drilling (LWD) and wireline well log suites collected at five sites; Mount Elbert, Iġnik Sikumi, Kuparuk 7-11-12 (all ANS), and 2L-38 and 5L-38 wells at the Mallik Research Site (Canada) includes more than 10,000 depth points, which was used for training, validation, and testing the ML models. The combinations of two or three well logs were found to be sufficient to predict the gas hydrate saturation at 80-90% accuracy against the NMR-derived gas hydrate saturations. The ML models trained and validated on data from three sites on ANS provide excellent qualitative prediction of gas hydrate content in the sediments at the Mallik site. The results indicate that the ML models trained on data from one basin can be successfully applied to predict key reservoir parameters in another basin. A generalized approach to select a well log combination leading to a better accuracy is discussed.

Keywords: machine learning; gas hydrates; well-logs; neural network

Corresponding author: E-mail: evgeniy.myshakin@netl.doe.gov. Tel: 412-386-5741

INTRODUCTION

Machine learning (ML) is an effective data-driven approach for both regression and classification (supervised or unsupervised) analysis of nonlinear systems. The systems can contain thousands of variables constituting a massive dataset for training with a random subset of data dedicated for independent validation. ML is particularly useful to assess problems and phenomena to which theoretical understanding is not complete and where empirical correlations and approximations are required. In the recent years the application of ML to geoscience problems has become a rapidly emerging field [1–3]. The important category of geoscience problems where ML can contribute is the spatio-temporal estimations of physical parameters that are difficult to monitor directly and/or sophisticated techniques are generally required for interpretation of measured data. Deep learning methods that use several hidden layers in artificial neural network (ANN) architectures are utilized to extract complex and highly non-linear features from the geoscience data [4, 5]. The supervised machine learning applies statistical learning to identify patterns in data and then makes predictions based on inferred patterns [6]. The term "supervised" refers to a set of samples where both the target output parameter (signal) and the predictive variables (well logs and derivatives of those logs) are known, such that the ML model is initially "supervised" by the known input and output before it is used to predict unknown targets. The data are split into a training set that serves to train a ML model against the known target parameter, and a testing set that represents an unbiased set of samples to assess the predictive performance of the trained model. This study is dedicated to application of supervised machine learning to predict key gas hydrate reservoir parameters in permafrost-associated accumulations.

Gas hydrate represents crystalline ice-like compounds where the gas molecules are included into the hydrate lattice comprised of water cages connected by H-bonding. Methane hydrate is widely diffused in permafrost areas and marine sediments. Recent U.S. Department of Energy and partner nation research suggests that methane hydrate is a promising future source of energy [7]. In recent years, a number of field-scale drilling and testing programs were

conducted at the Mallik research site in Northwest Canada [8], at the Mount Elbert [9], the Iġnik Sikumi [10], and the Kuparuk 7-1-12 [11] sites in Northern Alaska, in the eastern Nankai Trough offshore Japan [12], in the Bay of Bengal offshore India [13, 14], in the South China Sea offshore China [15], and in the Gulf of Mexico offshore the United States [16]. These programs were successful in confirming the technical viability of gas production from gas hydrate reservoirs through depressurization, understanding site-specific reservoir petrophysical parameters and details of the geological settings necessary to develop geological models for reservoir simulations. The petrophysical properties of gas hydrate reservoirs were inferred through seismic surveys, Logging-While-Drilling (LWD) and wireline well logs, plus depressurized and preserved core measurements. The production potential of a gas hydrate reservoir is mainly determined by the reservoir porosity, absolute permeability, *in situ* permeability, gas hydrate saturation (S_{gh}) in pore space in addition to initial pressure and temperature of that reservoir. S_{gh} is the parameter characterizing the amount of gas trapped in the hydrate lattice and that can be potentially released into a reservoir after the crystallographic structure of gas hydrate is decomposed. While most of those properties can be estimated directly in the field or in a laboratory using core samples, the evaluation of S_{gh} is a relatively complex process. The S_{gh} can be estimated using three physics-based methods that are based on the following: (1) electrical resistivity logs and the empirical Archie's law [17, 18], (2) processing sonic logs of compressional and shear velocities in the acoustic velocity method, and (3) NMR and density well-logs in the NMR-density porosity method, respectively. Each of these three methods are briefly discussed below; a detailed overview of these methods including their approximations and limitations can be found elsewhere [19].

1) Electrical resistivity method:

Gas hydrate acts as an electrical insulator and the gas hydrate-bearing sediments increases the resistivity of rock, which enables estimating S_{gh} using Archie's law [17, 18] that is used to assess mobile phase saturation in the pore space as follows:

$$S_w = \left(\frac{F*R_w}{R_t}\right)^{\frac{1}{n}} = \left(\frac{a}{\phi^m}\right)^{\frac{1}{n}} . \left(\frac{R_w}{R_t}\right)^{\frac{1}{n}} \quad (1)$$

where, R_t,R_{w} are log-measured resistivity of reservoir-rock saturated with all *in situ* fluids, and resistivity of connate water (without rock matrix), respectively. *F* is a formation factor, ϕ is porosity typically estimated from density logs, while a, m, n are empirical parameters; m is a function of rock cementation, n is a function of hydrate morphology, a is typically set to 1. Consequently, gas hydrate saturation, S_{gh} is calculated as 1 – S_w.

2) Acoustic velocity method:

In this method, acoustic velocities (compressional and shear wave velocities) are used to estimate S_{gh} using relationships that are either empirical [20] or based on rock-physics effective medium theory [21]. The acoustic velocity model requires a knowledge of mineralogy and bulk modulus that must be acquired through other means, and the assumption of gas hydrate morphology (the way how gas hydrate is precipitated in pore space in pore space).

3) NMR-Density porosity method:

This method based on the analysis of the transverse magnetization relaxation time (*T*2) of the hydrogen atoms that can differentiate between the water in the aqueous phase and the water belonging to the gas hydrate crystal lattice. The NMR logging tool measures porosity filled with aqueous phase (ϕ_{nmr}), whereas the density porosity tool (ϕ_{den}) measures total porosity, such that the difference between ϕ_{den} and ϕ_{nmr} is used to estimate S_{gh} [22–24] as follows:

$$S_{gh} = \frac{\phi_{den} - \phi_{nmr}}{\phi_{den}} \quad (2)$$

These three physics-driven methods discussed above are based on certain assumptions and empirical parameters that are not always well constrained and such constraints associated with these methods can be overlooked [19]. On the other hand, S_{gh} can be estimated through a supervised ML method by using a combination of well logs that bear a footprint of gas hydrate presence in a reservoir without making assumptions about the pore morphology and without any laboratory-estimated empirical parameters. That implies that the estimation of S_{gh} through ML is akin to an indirect measurement whose accuracy is dependent on the accuracy of the logs measured directly in the field and the S_{gh} dataset assigned during the training of the supervised

learning method. For instance, intervals of the wellbore, where its diameter (measured using the caliper log) either exceeds or shrinks beyond a certain threshold, can affect well log readings depending on the investigation radius of the logging tool. In such case the affected intervals are either assigned with corrections or removed from the original dataset.

In our previous work [19], we presented a generalized approach to predict S_{gh} through ML using well log information. For that, LWD well log suites from two wells on ANS, the Mount Elbert [9] and Iġnik Sikumi [10], provided the dataset for training and validation, and the NMR-derived S_{gh} along each depth was used as the target variable ("ground truth") in the supervised learning process. In that study, twelve different supervised ML algorithms belonging to five different classes were carefully examined against their ability to accurately predict the target variable and handle overfitting. Those classes were Ridge Regression [25] and its variants, Decision Tree [26] and its variants, k-Nearest Neighbor [27], ANN [28], and variants of Reduced Order Models[29, 30]. The results from that study revealed that Stochastic Gradient Descent Regression (SGDR) [31], the variant of Ridge Regression [25], and ANN [28] were the best algorithms with SGDR performance being more sensitive to the size of the training dataset. The accuracy of the best algorithms in predicting S_{gh} was ~84% that measured the accuracy of the fitted model in terms of the variation of predicted data set from its target values [19]. However, the ML models from the previous study were tested on a dataset constituting well log readings at the gas hydrate deposits belonging to the same basin. Thus, the applicability of the ML models deduced in the previous study [19] to other permafrost-associated gas hydrate accumulations in different basins remains unconfirmed. In this work, we investigate the capability of ML models to predict S_{gh} of any of the two basins (on ANS or in Northern Canada) based on the training of the ML models through well log datasets from five wells located in these two basins. The ML models were trained using the gas hydrate saturation values inferred by the NMR-Density porosity method, which is considered as the "ground truth" and helps in assessing the accuracy of ML-based predictions. The electrical resistivity method was also utilized to qualitatively confirm the presences of gas hydrate at corresponding depth points. The ML models are intended to complement the existed physics-driven methods discussed

above and serve as a tool to probe S_{gh} distributions at drilling sites with either a limited number of logs or compromised logs that preclude data interpretation using the conventional methods. One potential application of ML is using well logs available at hundreds of legacy wells located on ANS and in Northern Canada to predict gas hydrate saturation in those locations. Majority of those wells were drilled without intention to assess S_{gh}, but the ML method could utilize the available logs to indicate the presence of gas hydrate in those locations. The S_{gh} estimated using ML at locations where no exclusive measurements of S_{gh} are available extends our knowledge about gas hydrate occurrence in geological formations and provides data on a larger scale that can be a useful resource for geological and reservoir studies.

METHODOLOGY

The current study uses ANN to train ML models through dataset comprising various well log readings at depth intervals with and without gas hydrate reservoirs. In other words, the dataset includes non-gas hydrate-bearing units mainly comprised by shale as well as gas hydrate-bearing units mainly occurring in sandy-rich sediments. The workflow for a ML model preparation involves the following steps: (1) data pre-processing, (2) hyperparameter tuning, (3) well log combination optimization, and (4) model validation. The locations of five wells, i.e. the Mallik 2L-38 and 5L-38 wells in Northwest Territories, Canada, and Mt. Elbert, Iġnik Sikumi, Hydrate-01 (the Kuparuk 7-11-12 Site) on ANS are depicted in Figure 1. Well-log montages displaying downhole log data collected in those wells can be found elsewhere [32–36]. The following features (or well logs) relevant to this study are selected: bulk density (ρ), density porosity (ϕ), gamma radiation (GR), resistivity (R_t), compressional wave velocity (V_p), and shear acoustic wave velocity (V_s). For each depth point these six features correspond to a target variable (S_{gh}) known through the ground truth and also desired as output of the ML-trained model. Additionally, borehole diameters at different depths were available from caliper log and used as part of the outlier removal process.

The outlier removal was performed in a two-step manner: removal of data showing evidence of strong washouts and then removal of outliers based on the GLOSS algorithm [37] analyzing all features in the dataset. Washouts indicate enlarged sections of a wellbore where

the hole size is larger than the drill bit, which results in unreliable data readings from the borehole tools and compromises log data for that depth [38]. To mitigate washout effects, the data for each well was screened for large caliper values in the upper five percentile. The trimmed data was then scanned for outliers using the GLOSS algorithm that detects local subspace outliers using a global neighborhood search [37] by returning probability scores across features and depths instead of attempting to detect outliers within each feature separately. Table 1 lists the initial numbers of depth data points (each includes six features and a target value) and the numbers remaining after each step in the outlier removal procedure. The rule of thumb for ANN suggests that size of the training data should be at least 30 times the size of the weights [49], where the size of the weights in this study is defined by the number of well logs. Thus, for the six features the minimum size of the dataset should be 180 that is well below the sample size of the dataset used in this study, which is 5,392 and 3,915 samples for the wells in Northern Canada and on ANS, respectively.

To assess the accuracy of prediction in the validation process, the metric consists of the coefficient of determination (R^2) or the accuracy score, which is calculated using Equation 3. This accuracy score was used in our previous works [19], and has been used in other studies, for e.g. assessing porosity distribution with ANN [39].

$$R^2 = 1 - \frac{\sum_i (y_i - \hat{y}_i)^2}{\sum_i (y_i - \bar{y})^2} \qquad (3)$$

where y_i, $\hat{y}_i$, and $\bar{y}$ are the expected value of S_{gh} ("ground truth"), a predicted one, and average expected S_{gh}, respectively. The ideal R^2 value is 1 while any deviations of predicted values for expected ones result in a R^2 value below 1. The "ground truth" are taken as values of the NMR-derived S_{gh} which are confirmed by the electrical resistivity method. In other words, the electrical resistivity method should confirm the presence of gas hydrate at a particular depth if a NMR-derived S_{gh} value is accepted as "ground truth" at that depth. Using NMR-derived S_{gh} as the "ground truth" is a common practice used by others to assess the accuracy of other methods; electrical resistivity and acoustic velocity methods [22, 40, 41].

To account for the variability in performance of ML algorithms due to sample sizes used for training, cross-validation was performed using the k-fold method where k-1 sets are

randomly chosen as training sets while a single set is used for validation. The k-fold cross-validation allows k different combinations of training and validation data and the average of accuracy scores from k different rankings is used to assess cross-validation. k equal to 2-5 was found to be sufficient to maintain model consistency in predictions. Generally, it is considered that 80/20 or 70/30 splits, where at least 80% or 70% of data are used for training, are sufficient to ensure the training of the ML models and provide highest accuracy in predictions. For this study, it was determined that 80/20 was an appropriate split based on similar studies that also employed well-logs with ML, for e.g. Song et al. [42]. The 20% of the data that is to be used for validation purposes was not fixed and could belong to different wells each time a ML model is trained.

Each feature was normalized based on the minimum-maximum values of that feature (well log), which is done to ensure the loss function is not adversely impacted by any large magnitude in the input data; specifically, normalization of the data helps make the computations relatively more efficient through faster convergence, but it may not necessarily improve the accuracy of the trained model. Various combinations of features were taken to train a ML model to predict the target variable. Before a ML model can be applied to a selected dataset, the hyperparameters of the algorithm must be tuned for optimal performance because, unlike the weights of the ANN, the hyperparameters are not optimized during the supervised learning process. More specifically, hyperparameters are non-trainable static parameters that affect the training procedure and a ML model quality, which means the tuning of hyperparameters must be done prior to training the ML model. To find an optimal set of hyperparameters, a global grid search method was used that entailed testing the accuracy of each discrete value combination of hyperparameters. For each set of hyperparameters, a ML model was trained and validated using all six features available in the dataset. The Adam optimizer for the stochastic gradient descent algorithm and the mean squared error as the loss function were utilized. Such choice is typical in the recently reported machine learning work in classifying wireline log shapes [42] and real-time well log predictions [43]. The neural network topology involves a number of hidden layers, where each layer is composed of several nodes

(also called neurons), such that the nodes on each layer connect the layers per the activation function. Among different mathematical forms of activation function, it has been found that rectified linear unit (ReLU) works well for vast majority of regression problems; therefore, ReLU is used for the hidden layers, while final output layer uses the linear activation function. After each hidden layer, a dropout layer was included in order to prevent overfitting. Dropout is a regularization method where nodes are randomly excluded during the training process to prevent certain nodes from dominating the prediction pattern. The frequency of node exclusion is called the dropout rate and it was set at 0.5 [44] in this study. The remaining hyperparameters are also tunable to ascertain the optimal training procedure: number of hidden layers, number of nodes per layer, learning rate of the optimizer, batch size, and epochs. Batch size refers to the interval of data points processed before the trainable parameters are updated, and epochs are the number of times the entire training set is used. We perform a broad tuning first with learning rates ranging from 0.0001 to 0.01, two to three layers, 10-50 nodes per layer, 100-500 batch size, and 100-500 epochs. After observing the hyperparameters that consistently lead to high R^2 on the testing data, fine tuning was performed by fixing those hyperparameters and grid searching smaller increments in other hyperparameters. A typical grid search for four hyperparameter involving their respective ranges is depicted in Figure 2. The optimal values of hyperparameters for ML models trained using ANS wells include two hidden layers with 40 nodes per layer, 0.001 learning rate, 100 batch size, and 500 epochs. Similar hyperparameters tuning process for ML models trained using Mallik wells resulted in the same optimal values of hyperparameters.

RESULTS AND DISCUSSION

A brief summary of the results obtained in this study is given below:

- R^2 distributions show that addition of a third feature into a well log combinations (WLC) improves the accuracy of ML models;

- ML models trained using three well-logs from ANS (ϕ, Rt, V_p) predict S_{gh} at the Mallik site with an excellent accuracy ($R^2 > 0.90$) and;
- ML predictions of S_{gh} are excellent in the range where S_{gh} values above 50%, while ML predictions in the lower range of S_{gh} are substantially underestimated;
- Pearson's descriptive statistics was utilized to identify a better WLC and a realization for a "blind well" where no "ground truth" is available.

ML models utilizing various WLC

In this study, features of the ML model are selected from the above-mentioned six well log inputs, and the selected features are referred to as well log combinations. To ascertain variance in predictions of the target variable, each ML model was trained and validated one hundred times. That produces 100 *Sgh* predictions (realizations) and R^2 values for each WLC. Those *Sgh* predictions are not the same because of randomly initialized *weights* for every layer in ANN for a ML model [45]. The R^2 values are then used to calculate an average R^2 that enables ranking the ML model performance per each WLC. The ML models using a single well log, WLC with two and three well logs were used for comparative performance analysis. We intentionally limit the number of well logs in various WLC to three in order to achieve acceptable accuracy in prediction with fewer number of well logs, especially because a ML model utilizing a fewer number of well logs can be applied to a larger number of geological formations, where only a limited number of well logs may have been acquired.

To evaluate performance, first the models with only a single feature are considered. This allows narrowing down the well log variables per their accuracy in predicting S_{gh} as a single independent feature. Table 2 displays the average R^2 values for the models utilizing only a single feature that were trained and validated for the Mallik and ANS wells, separately. Following our previous works, the model providing accuracy above 80% was considered successful [19]. The average R^2 values indicate that models using acoustic (V_p, V_s) or resistivity (Rt) well logs provide distinctly high scores compared to the remaining well logs. This is expected given that Rt and (V_p,V_s) are sensitive to the presence of gas hydrate and these logs serve as data source to predict S_{gh} in the electrical resistivity and acoustic velocity methods,

respectively. In Table 2, the R^2 values were calculated for the ML models validated on the same wells, within the same basin. The attempts to predict S_{gh} at the Mallik or ANS wells using ANS-trained or Mallik-trained ML models, respectively, with acoustic or resistivity logs result in poor R^2 (not shown). In other words, ML trained models with a single well log does not perform reliably when used to predict S_{gh} using "unseen" or "blind" data at wells in another basin.

Next, all WLC pairs were sampled to train respective ML models, validate them using the well log data at the same basin, and test them on the "blind" wells belonging to another basin. Table 3 shows results for pair WLC with R^2 above 0.20. It is evident from R^2 values that using two features improves the accuracy of the ML models within the same basin where R^2 is over 0.9. Application of the ANS-trained and Mallik-trained models to predicting S_{gh} at Mallik and ANS wells, respectively, as "blind" wells (not participating in training and validation processes) lead to declined performance. Among the two models trained using Mallik and ANS wells, respectively, the ANS-trained ML model provides better accuracy in predicting the target variable at a blind well (the Mallik wells) compared to using Mallik-trained ML model in predicting the target variable at a blind well (ANS wells). This variability in performance between the two models trained using datasets from two different basins can be attributed to the fact that Mallik-trained ML models are based on the data available at one location, while ANS-trained ones include data available from three different sites (Figure 1). Using the database that includes three locations with variability in their rock properties, the ANS-trained ML models can capture that variability in gas hydrate hosting sediments (mineralogy, grain size, etc.) that show broad range of saturations. In other words, the variability exhibited by the ANS dataset is learned by the ML model that enables it to predict gas hydrate occurrence in natural environment more robustly than the Mallik-trained model. Table 3 indicates that ANS-trained ML models based on (*GR,* V_p) and (*Rt,* V_p) pairs provide excellent predictions (average $R^2 > 0.84$) for S_{gh} at the Mallik site. The (*GR,* V_p) pair is important from practical standpoint since *GR* is the one of the most primary logs that is acquired to characterize a formation in terms of its sand-shale geology, which means that *GR* log would be most likely available for almost all the legacy wells. The *GR* log can be used to differentiate sandy silt or silty sand intervals, potential

candidates to host pore-filling concentrated gas hydrate accumulations, from more finely sorted clay-rich intervals. In combination with the sonic tool readings, the *GR* log enables predicting S_{gh} by trained ML models that is similar to NMR-quality S_{gh} prediction. Notably, Saputro et al. [46] also found that *GR* and V_p are critical features in applying ANN to predict porosity log data with R^2 reaching 0.937.

The features that appear in the highest performing pair WLC (Table 3) were selectively augmented with an additional feature to produce triplet WLC in attempt to further improve the accuracy of the ML models. Since V_p appears in all top pair WLC performers (Table 3), therefore it is preserved in the sampled triplet WLC. Table 4 lists the average R^2 of triplet WLC selectively sampled based on pair WLC results from Table 3. Compared to pair WLC, the addition of the third feature does not significantly improve the R^2 when the trained models are validated against the data within the same basin. However, there is an improvement in the R^2 values when the models are tested to predict S_{gh} at the sites in another basin. For example, there is only two pair WLC performers providing R^2 above 0.80 for the models tested at the Mallik wells, while there are six such triplet WLC performers. Noticeably, two WLCs including (ϕ, *Rt*, V_p) and (ϕ, *GR*, V_p) lead to ANS-trained ML models giving the higher R^2 values to the "blind" Mallik wells compared to the R^2 values deduced from the validated data sets (Table 4). The general trend of better performance of the ANS-trained ML models in predicting the target variable at the "blind" Mallik wells is preserved for the triplet WLC. The reason additional logs improve the predictions from a different basin is intuitive in the sense that adding additional logs enable the ML model to better capture the signatures of the formation that control S_{gh}, which means that complete signatures controlling S_{gh} are unlikely to be present in a single log; this hypothesis is also supported by the physical knowledge of gas hydrate deposits that are known to be affected by various characteristics of the formation that is measurable using well logs.

R^2 Distributions

The performance of the ML model is measured using an averaged R^2 value, which is a metric of accuracy, and evaluated using R^2 distributions, which provide precision or consistency

in predictions. Tables 2-4 collect the average R^2 values illustrating the accuracy of ML models in predicting the target variable. Figure 3 depicts the R^2 distributions for ANS-trained ML models for the three WLC including *Vp*, (*Vp* and ϕ), and (V_p, ϕ, and *GR*). Figure 4 shows the R^2 distributions for Mallik-trained ML models using the same WLC sequence. The figures demonstrate that consequent addition of a feature into a WLC improve average R^2, although it does not always lead to increase in prediction accuracy, or in other words there is no clear consistency between improvement in R^2 and improvement in prediction. As an example, the distribution of R^2 for Mallik-trained ML models using the triplet WLC appears to be broader than those utilizing the pair WLC. The addition of ϕ to V_p leads to decrease in accuracy for ANS-trained ML models when applied to the 2L-38 well, however, further augmentation of the ϕ and V_p pair with *Rt* increases the R^2 value over 0.90, similar to 5L-38 (Tables 3 and 4). The corresponding R^2 distributions are narrowed down and yielded high R^2 values exceeding the value obtained using the validation sets (Figure 3). The similar trend is obtained when *GR* is added to the pair instead of *Rt* (Figure S1a in Supplementary Materials). However, using V_s instead of *Rt* does not improve the R^2 for 2L-38 (Figure S1b).

A somewhat different pattern emerges after examining the trend for Mallik-trained ML models (Figure 4). The models are noticeably robust and accurate with single feature (V_p) and (V_p, ϕ) pair when Hydrate-01 is used as a "blind" well, however, a triplet WLC is required to reliably predict S_{gh} when Mt. Elbert and Ignik Sikumi are used as "blind" wells. The addition of *Rt* to (V_p, ϕ) WLC creates distinguishable distributions for each ANS well (Figure S2a) with Hydrate-01 achieving closest accuracies with Mallik-trained models. Although the average R^2 increases when *Rt* is used instead of *GR*, the R^2 distribution becomes wide, indicating deterioration in predictions from the Mallik-trained models for those wells. Figure S2b shows that relplacing *Rt* with V_s in the triplet WLC improves the consistency but sacrifices the accuracy. Thus, the ANS-trained ML models are achieving narrower distributions and higher R^2 than the Mallik-trained ones, which is likely due to larger variability captured by the training data from three wells at different locations in the case of ANS-trained model compared to the training data from two wells at one site for the Mallik-trained model. Tradeoff between

precision and accuracy due to removal or addition of features in the WLC impacts the Mt Elbert and 2L-38 wells the most; this is likely due to the quality or quantity of the key feature impacting gas hydrate saturation for the respective wells.

Gas hydrate saturation prediction

The average R^2 values collected in Tables 3 and 4, and R^2 distributions shown in Figures 3 and 4 characterize the performance of ML model. Those values and distributions of R^2 were created using 100 S_{gh} predictions compared to the "ground truth" of S_{gh}. The predicted S_{gh} values with the highest R^2 were used to select the ML models. Figure 5 shows predicted *vs* expected ("ground truth") S_{gh} scatter plot for the triplet WLC (ϕ, *GR, Vp*), where the straight line with unit-slope represents the perfect match. The figures demonstrate the formation of two distinct clusters of data (highlighted by ovals), where the first cluster indicates accurate predictions at high gas hydrate saturations, and the second cluster designates the predictions underestimating the expected values at low S_{gh} (<0.5). A similar pattern is found in predictions using other WLC (Figure S3). It is reasonable to say the main source of deviation of R^2 from a perfect value of 1.0 is due to poor prediction of S_{gh} at lower range (S_{gh}<0.5). This is an interesting result that may be exhibiting the shortcoming in the NMR method in reliably predicting S_{gh} at lower range (S_{gh}<0.5). Consistent under-prediction for S_{gh} < 0.5 by ML models utilizing different WLCs is an indication of systematic lack in quality of the original "ground truth" data in those lower range of gas hydrate saturations. One could argue that under-prediction for S_{gh} < 0.5 by ML models could also mean shortcoming of ML to match the data at lower Sgh, however, there is no rationale that explains this shortcoming in ML. The hypothesis about the shortcoming in the NMR mentioned above is discussed in detail below.

In a recent development of the NMR-based method, the longitudinal relaxation time, T_1 and transverse relaxation time, T_2 distributions are jointly inverted, compared to conventional processing, which inverts a T_2 distribution from the echo signal using a constant T_1/T_2 ratio [24]. According to the study, using the constant T_1/T_2 ratio causes the NMR porosity in gas hydrate bearing zones to be underestimated by about 3–6 porosity units, and the derived gas hydrate

saturations to be overestimated by ~8–10%. This indicate that the predicted *vs* expected S_{gh} values in Figure 5 should experience a bias towards higher expected S_{gh} values. This is confirmed using Figures 5 and Figure S3 that show the data clusters corresponding to high S_{gh} values lying below the unit-slope line, which is a line depicting perfect match; this means that the expected S_{gh} values obtained by the conventional NMR processing are systematically higher than the predicted values. Figure 6 and Figure S4 show the comparison of predicted and expected S_{gh} values (*vs* depth) for select wells and ML models, where many intervals corresponding to high S_{gh} clearly show that the expected values are higher the predicted S_{gh}.

The overestimation of conventional NMR-derived S_{gh} by 8-10% cannot fully explain large underprediction of S_{gh} at the lower range (S_{gh} <50%) (Figure 5 and Figure S3). To elaborate further, it should be recalled that the degree of gas hydrate saturation is strongly controlled by reservoir quality, such that a lower-quality reservoir may be maximally-saturated at 50%. In contrast, higher-quality reservoirs can achieve saturations above 80% [53]. A lower-quality reservoir implies more finely sorted particles, more clay, silt and mud content, and is typically characterized as silty clay or clayey silt facies. Thus, the sediment bearing low gas hydrate saturations are enriched with clay such as illite, kaolinite, chloride, smectite-family, and others. Recently, Elsayed et al. [47] reported the effect of clay content on the spin−spin NMR relaxation time measured in porous media, such that the increase in oscillating magnetic pulses (TE spacing) leads to strong reduction in T_2 distribution (tails <0.1 ms) due to clay-induced internal field gradients. Consequently, if using a conventional technique, interpretation of T_2 distribution causes underestimation of NMR-based porosity, implying that the NMR-derived gas hydrate saturation will be overestimated in case of gas hydrate in clay-rich sediments. This can be a leading factor responsible for discrepancy between NMR-derived S_{gh} and ML-derived S_{gh} at many depths where S_{gh} values fall lower than 50%. In such locations, the low S_{gh} in pore space generally occur in sediments with elevated clay content that would cause the excessive assignment to S_{gh}.

It can be argued that a thorough analysis of S_{gh} predictions by the ML models with feature engineering by considering various WLC can potentially reveal the shortcomings of a

first principles-based method (e.g. NMR-density porosity method) that has been used to measure the "ground truth" of S_{gh}. It should be emphasized that the combinations of features are required in the training process to identify potential limitations of "ground truth" data. This potential capability separates a ML model from a physics-driven method that typically utilizes a parametric analytical equation(s) to connect a feature of interest with a target variable. To understand the limitation of a physics-driven methods that are typically applied in characterization of core samples, critical analysis of parameters and equation forms are generally needed.

It must be noted that for systems with moderate complexity, such as pure fluid dynamics without the complexity of geological formations, first principles-based models are sufficiently accurate to depict their behavior. However, for complex systems, such as gas hydrate deposits or multiphase flow in porous media, first principles-based models may not be accurate enough to depict behavior of such complex systems. In such systems, directly-measured features (e.g. well logs) are better representation of the underlying correlations with the target variable (S_{gh}) than the first principles-based models (e.g. S_{gh} based on NMR-derived model), therefore, combining feature engineering (e.g. selective WLC) with data-driven ML appears to be a more accurate representation of S_{gh} than NMR-derived model that is considered the ground truth. The improved performance exhibited by ML combined with feature engineering over first principles-based models is also exhibited by other studies with relatively complex systems, such as fluid flow characterization in pipes/wells [48, 49], PVT modeling of complex fluids [50], etc. The improved performance of ML combined with feature engineering over first principles-based models for relatively complex systems as observed in this study and also confirmed by others [48–50] suggest that variability represented in first principle-based features (e.g. well logs measured based on fundamental properties) and their appropriate combination when used with ML enables more accurate prediction of target variable than possible through first principles-based models.

Selection of WLC for a "blind" well

In the previous section, it was determined that triplet WLC should provide reliable prediction of the target variable using ANS-trained ML models (Table 4). Depending on the number of LWD or wireline well logs available at a site of interest, there could be several combinations of logs constituting triplet WLC. A trained ML model applied to a "blind" well with a triplet WLC as input would predict a realization of S_{gh}. One hundred such applications provide 100 realizations. Without "ground truth" knowledge to assess the accuracy of prediction through R^2 values, the remaining statistical metrics to characterize those realizations is precision. Precision indicates how close those S_{gh} predictions are to each other and for ML applications where "ground truth" is known it visually manifests itself through the spread of R^2 values. In case where "ground truth" (and R^2 values) is not known, another metric should be utilized.

To quantify the precision of realizations obtained from an ANS-trained model using a triplet WLC, Pearson's correlation coefficients were calculated for each of those 100 realizations against the remaining 99. The Pearson's correlation coefficient (r_{xy}) between two realizations x and y is estimated using Equation (4) below:

$$r_{xy} = \frac{\sum_{i=1}^{n}(x_i - \bar{x})(y_i - \bar{y})}{\sqrt{\sum_{i=1}^{n}(x_i - \bar{x})^2}\sqrt{\sum_{i=1}^{n}(y_i - \bar{y})^2}} \qquad (4)$$

where, n is a realization size (2,472 depth points at the Mallik 2L-38 well); x_i and y_i are individual S_{gh} predictions at a depth point; $\bar{x} = \frac{1}{n}\sum_{i=1}^{n} x_i$ (the realization mean) and $\bar{y}$ is analogous to $\bar{x}$. r_{xy} is a measure of correlation between 0.0 (no correlation), and 1.0 (identical realizations). Each realization has 99 correlation coefficients, which are processed to obtain mean and median values. The sums of all averaged coefficients are defined as "scores" that constitute the metric to assess the precision of those realizations.

To identify a triplet WLC leading to better reliability in predicting S_{gh}, the triplet WLC reporting best precision (best "scores") is recommended to be selected. That recommendation is based on the analysis of R^2 distributions depicted in Figures 3-4 and S1-2. As a general trend, triplet WLC providing high averaged R^2 value (accuracy) also deliver high precision showing narrow spreads of individual one hundred R^2 values. Therefore, selecting a WLC with high

precision most likely results in reliable estimates of the target variable. To present an instructive example, the ANS-trained ML models using the following triplet WLC; *(ϕ, GR, Vp)*; *(ϕ, Rt, Vp)*; *(ϕ, Vp, Vs)* were selected to predict S_{gh} at the Mallik 2-38L well. The R^2 distributions are depicted in Figures 3c, S1a, and S1b, respectively. Their corresponding averaged R^2 values are 0.8179, 0.9038, and 0.5839 (Table 4). Those figures and numbers clearly show that better averaged R^2 is accompanied with more narrow distribution of R^2 values.

Figures 7 and S5 show the averaged Pearson's correlation coefficients for select triplet WLC together with standard deviations for the mean values. In Figures 7 and S5, the median lines consistently appear above the mean, thus indicating correlation coefficients are grouped toward high values. The scores are depicted in Figures 7 and S5 and Table 5 together with other descriptive statistics. Comparison of scores with averaged R^2 values reveals the triplet WLC that provides the best performance demonstrated by the highest "scores" (Table 5). In other words, for a "blind" well, which provides well logs "unseen" by the ANS-trained ML models, the "scores" based on Pearson's correlation coefficients can be used to assess a triplet WLC performance with respect to the target variable.

Table 5 also collects information about the Pearson's coefficients for realizations providing R^2 values closest to averaged R^2 values and R^2 values for realizations providing maximum Pearson's coefficients. Comparison of those numbers allows to deduce that the selection of a realization with the highest Pearson's coefficient most likely leads to a prediction with a R^2 value on the right tail of a R^2 distribution. That concludes the suggested screening approach to first select a top triplet WLC performer and then pick a suitable realization based on Pearson's statistics. It should be emphasized that the approach would not guarantee selection of the best WLC among performers delivering close averaged R^2 (like 0.90 and 0.91), but it does filter out WLC performers with poor averaged R^2 (like 0.60). Similarly, choosing a realization with the maximum Pearson's coefficient would not guarantee selection with maximum R^2 value, but most likely the realization would have R^2 higher than average R^2.

Further development

The ML models considered above were trained using either ANS or Mallik well logs to predict the target variable at the Mallik site or ANS wells, respectively. Obviously, training a ML model using well logs from all five wells on ANS and at the Mallik site can bring even higher accuracy for a "blind" well compared to that computed for the ANS-trained models. Such models were trained following the approach described in the Methodology section of this report, and the validation step has shown consistent accuracy with R^2 above 0.9. These ML models are reserved for our further study to analyze logs available at legacy wells located on ANS and in Northern Canada. Data provided by hundreds of industry wells has confirmed that gas hydrate exists widely on the North Slope both within and below the permafrost section and is almost exclusively contained within the sand-rich units [23, 51]. These legacy wells were drilled without an intention to assess S_{gh} and were mainly associated with oil exploration activity at formations deeper than the gas hydrate stability zone. Access to the routine well logs such as ϕ, *GR*, and readings from sonic and/or electrical resistivity tools would open up a possibility to screen for gas hydrate presence at those locations and help refine our knowledge about gas hydrate reserves in North America.

The presence of acoustic logs in the top WLC performers (Table 3) is a promising sign that can be used towards 3D gas hydrate reservoir characterization using ML in future. Such models can utilize surface seismic and VSP data to connect the attributes extracted from those surveys with acoustic well logs through ML training. The ML models can provide a means to evaluate high-resolution acoustic data in the lateral direction from the vertical wellbore and use them to get detailed S_{gh} spatial distribution.

The ML models presented in this study are applicable to permafrost-associated continuous sandy-rich accumulations typically characterized with high porosity and absolute permeability. To provide the ML model's application to marine gas hydrate-bearing sediments and/or gas hydrate sitting in fractures and veins, a training database should be extended with corresponding suites of well logs at locations of interest. However, the potential of ML in characterizing marine gas hydrate since gas hydrate in marine sediments often occurs in interbedded stratigraphic units where thin mud layers with no gas hydrate alternate with gas

hydrate sandy sections. This variability in mud/sand facies at a resolution that can be finer than the resolution of the well logging tool could lead to averaging of the facies properties by well logs, thereby leading to a poorly characterized target property of closely spaced layers with different lithology [52]. Furthermore, the "ground truth" data used to train the ML models should be scrutinized and, if possible, compared with core laboratory measurements. The physics-driven methods like the NMR-based one that proved to provide reliable estimates for high *Sgh* in high-quality reservoirs might not deliver correct saturation values for fracture-filled gas hydrate and/or gas hydrate in thinly interbedded sedimentary sections.

Conclusions

The ML models trained using the ANS well logs in the Eileen Gas Hydrate Trend were successfully applied to predict gas hydrate saturation distribution at the Mallik 5L-38 and 2L-38 wells in the Mackenzie Delta Basin (Canada). The pair of well logs comprising compressional velocity with gamma ray or electric resistivity readings provide high prediction accuracy (measured through R^2 above 0.82) relative to NMR-based gas hydrate saturations. Adding density porosity to those two pairs can further improve the accuracy by obtaining R^2 up to a 0.92 value. The ML models trained using Mallik wells were also tested to predict gas hydrate saturations at the ANS wells; Mount Elbert, Iġnik Sikumi, and Kuparuk 7-11-12. The accuracy of the best ML model using density porosity, electrical resistivity, and compressional velocity logs was within the range of 0.72-0.76. The better performance of the ANS-trained ML models over the Mallik-trained ones was attributed to the nature of the training datasets. In the former case, the information was collected from three locations on ANS capturing more variability in geological settings compared to only one site in the latter case. The analysis of predicted values against the "ground truth" indicates an excellent match when gas hydrate saturations are above 50%, while for the lower values of gas hydrate saturation the predicted values are underestimated. It is speculated that this finding points out at a potential problem in the interpretation of NMR-logs to deduce S_{gh} values for poor quality reservoir intervals.

ML models using all five wells were trained for further application at sites without prior knowledge of gas hydrate distribution in reservoir units. The models were validated showing consistent accuracy with R^2 above 0.9.

The trained ML models utilize various triplet WLC comprised of density porosity, gamma ray, acoustic velocities, and electrical resistivity logs. Without prior knowledge of "ground truth" a generalized approach was developed to select which of those triplet WLC provides one of the top performances at a "blind" well. The approach is based on the descriptive statistics collected using one hundred realizations to predict gas hydrate saturations at every ML model.

Acknowledgement

This work was performed in support of the U.S. Department of Energy's Fossil Energy Crosscutting Technology Research Program. The research was executed through the NETL Research and Innovation Center's Hydrate Research Field Work Proposal. This research was supported in part by an appointment to the National Energy Technology Laboratory Research Participation Program, sponsored by the U.S. Department of Energy.

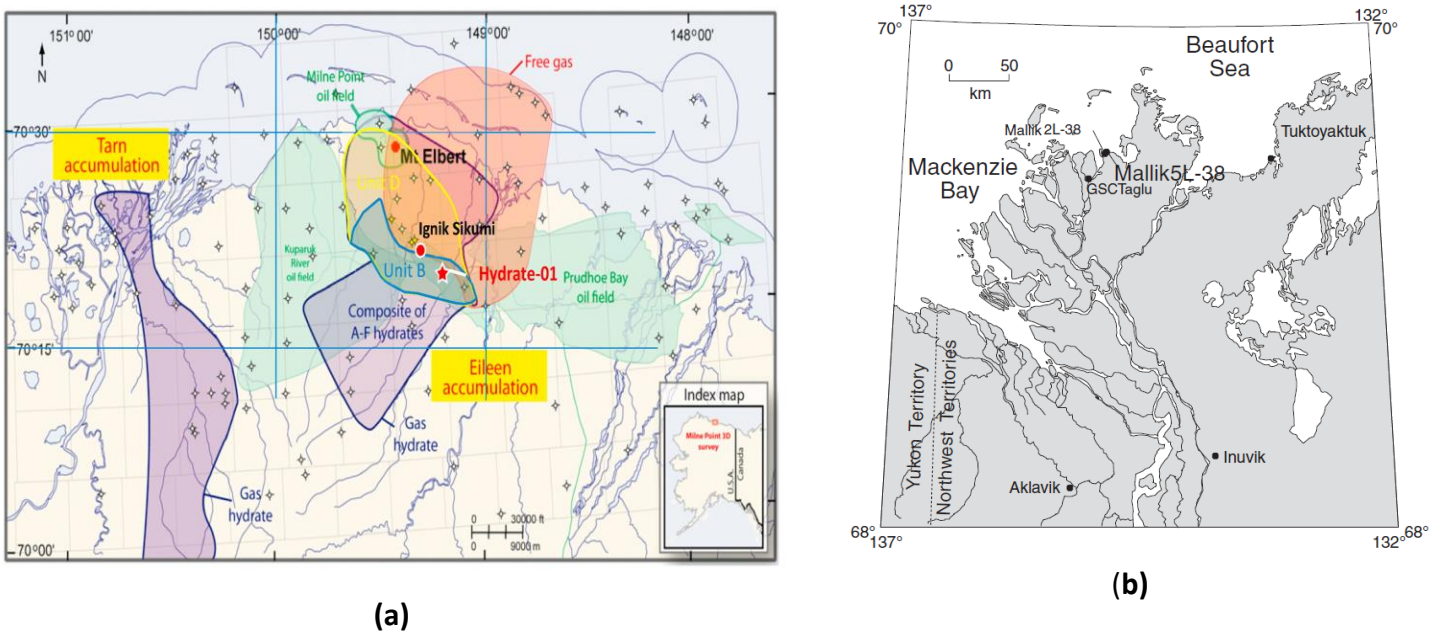

Fig. 1 (a) Location map of ANS regions showing Mt. Elbert, Iġnik Sikumi, and Hydrate-01 well locations in Eileen gas hydrate accumulation [53]. (b) Location map of the Mackenzie Delta region showing the Mallik 2L-38 and 5L-38 drilling sites [54].

Table 1 Numbers of depth data points for each well before and after outlier removal

Well	**5L-38**	**2L-38**	**Mt Elbert**	**Iġnik Sikumi**	**Hydrate-01**
Basin	Beaufort-Mackenzie		Eileen Gas Hydrate Trend		
Initial Data	3120	2639	822	1127	2236
After Caliper Screening	2964	2507	778	1070	2124
After GLOSS algorithm	2920	2472	771	1053	2091

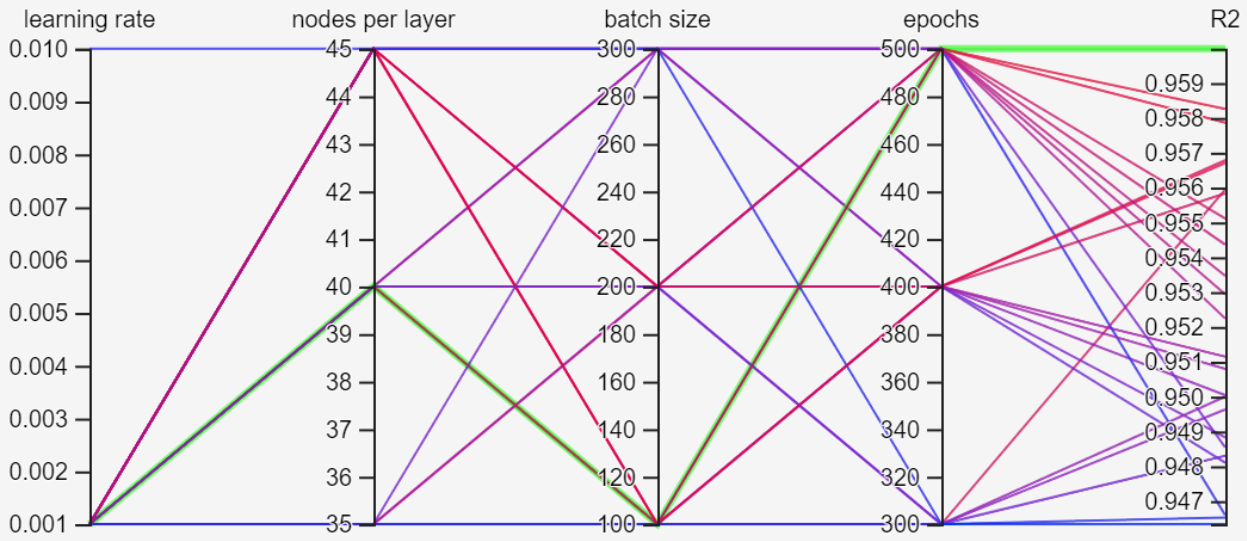

Fig. 2 Tensorboard parallel coordinate view of hyperparameter fine tuning two-layer neural networks showing R^2 and their corresponding hyperparameters. The green line represents a ML trained and validated model with the highest R^2.

Table 2 Average R^2 for ML models trained and validated using single logs

Feature	**Mallik trained and validated**	**ANS trained and validated**
Vp	0.8487	0.7608
Rt	0.7937	0.7712
Vs	0.7755	0.5249
GR	0.1289	0.4139
ϕ	0.0974	0.2372
ρ	0.0829	0.3367

Table 3 Average R^2 for ML models trained, validated, and tested using pairs of well logs.

	Mallik trained				**ANS trained**		
WLC	**Mallik validated**	**Mt Elbert tested**	**Ignik Sikumi tested**	**Hydrate-01 tested**	**ANS validated**	**5L-38 tested**	**2L-38 tested**

ϕ *Vp*	0.9239	0.3604	0.5523	0.8264	0.8666	0.9330	0.5438
GR Vp	0.9116	0.4743	0.6166	0.8274	0.8504	0.8559	0.8918
Vp Vs	0.8969	0.2903	0.4153	0.7778	0.8491	0.7157	0.6505
Rt Vp	0.8964	0.3518	0.5111	0.6842	0.8588	0.8676	0.8370
GR Vs	0.8418	0.2020	0.4401	0.7233	0.6684	0.7247	0.7719

Table 4 Average R^2 for ML models trained, validated, and tested using triplets as WLCs

	Mallik trained				**ANS trained**		
WLC	**Mallik validated**	**Mt Elbert tested**	**Ignik Sikumi tested**	**Hydrate-01 tested**	**ANS validated**	**5L-38 tested**	**2L-38 tested**
ϕ *Rt Vp*	0.9505	0.7436	0.7569	0.7205	0.8833	0.9234	0.9038
GR Rt Vp	0.9417	0.7589	0.6768	0.5447	0.8794	0.8196	0.8243
ϕ *GR Vp*	0.9352	0.3912	0.5785	0.8321	0.8780	0.9115	0.8179
ϕ *Vp Vs*	0.9289	0.4199	0.5849	0.8288	0.8919	0.8845	0.5839
Rt Vp Vs	0.9249	0.7109	0.6319	0.6075	0.8854	0.8482	0.8402
GR Vp Vs	0.9128	0.5083	0.6412	0.8262	0.8814	0.8235	0.8887

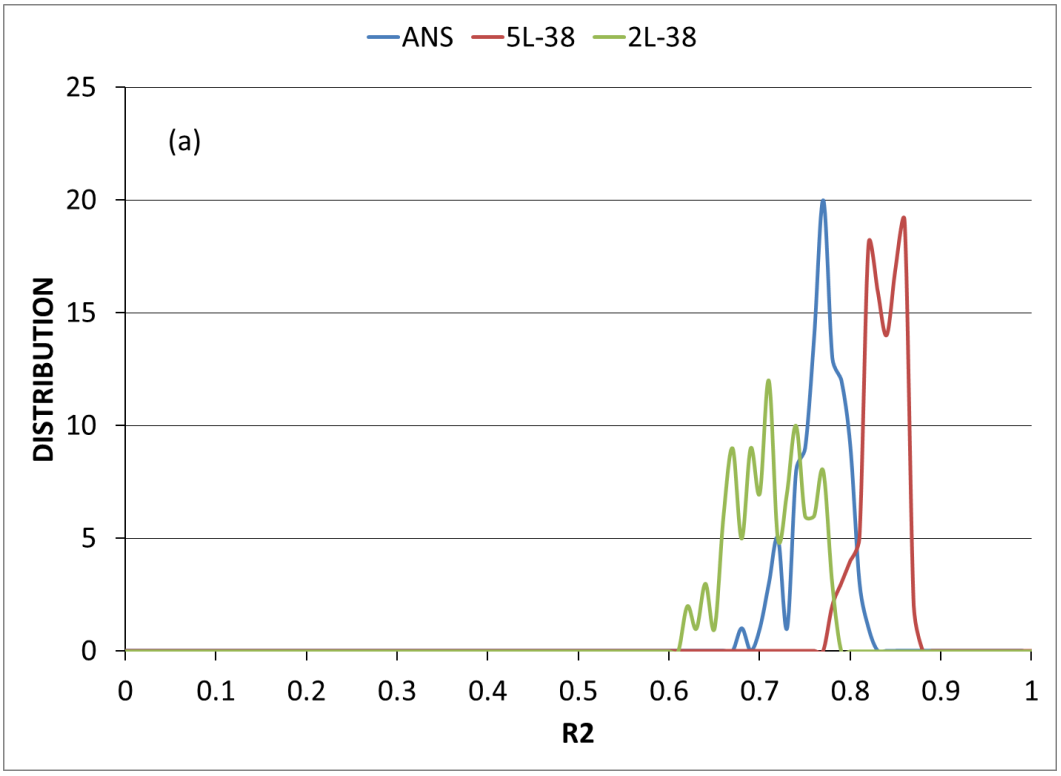
ANS
5L-38
2L-38
(a)
DISTRIBUTION
25
20
15
10
5
0
0
0.1
0.2
0.3
0.4
0.5
0.6
0.7
0.8
0.9
1
R2

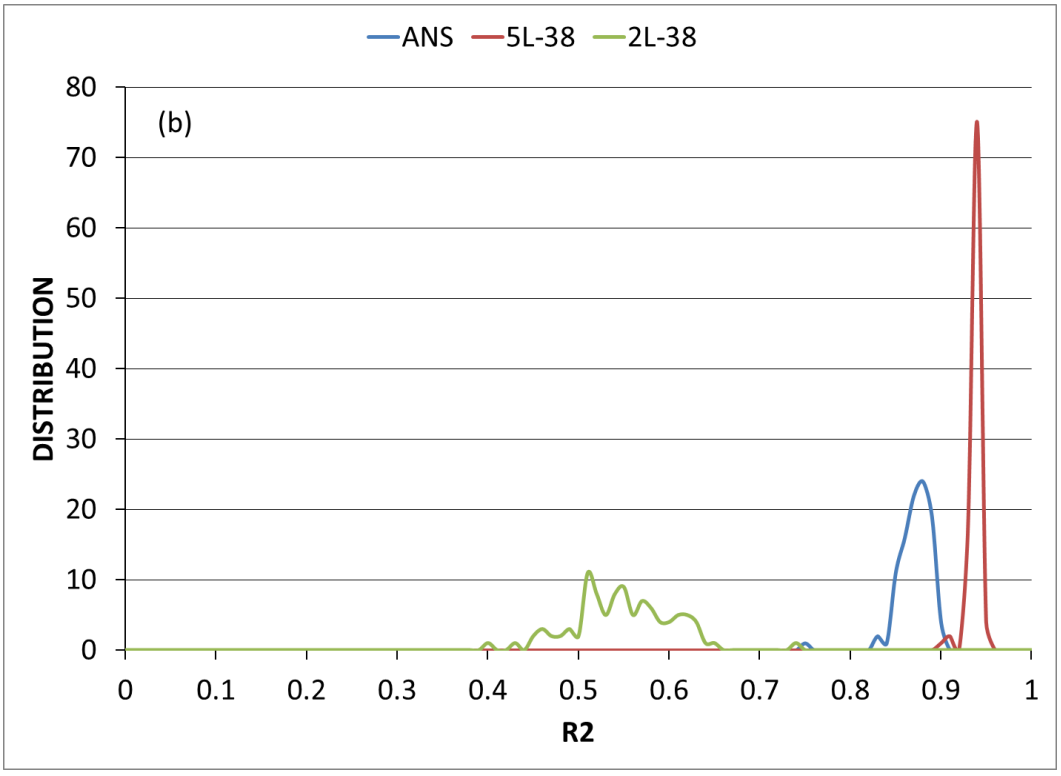
ANS
5L-38
2L-38
(b)
DISTRIBUTION
80
70
60
50
40
30
20
10
0
0
0.1
0.2
0.3
0.4
0.5
0.6
0.7
0.8
0.9
1
R2

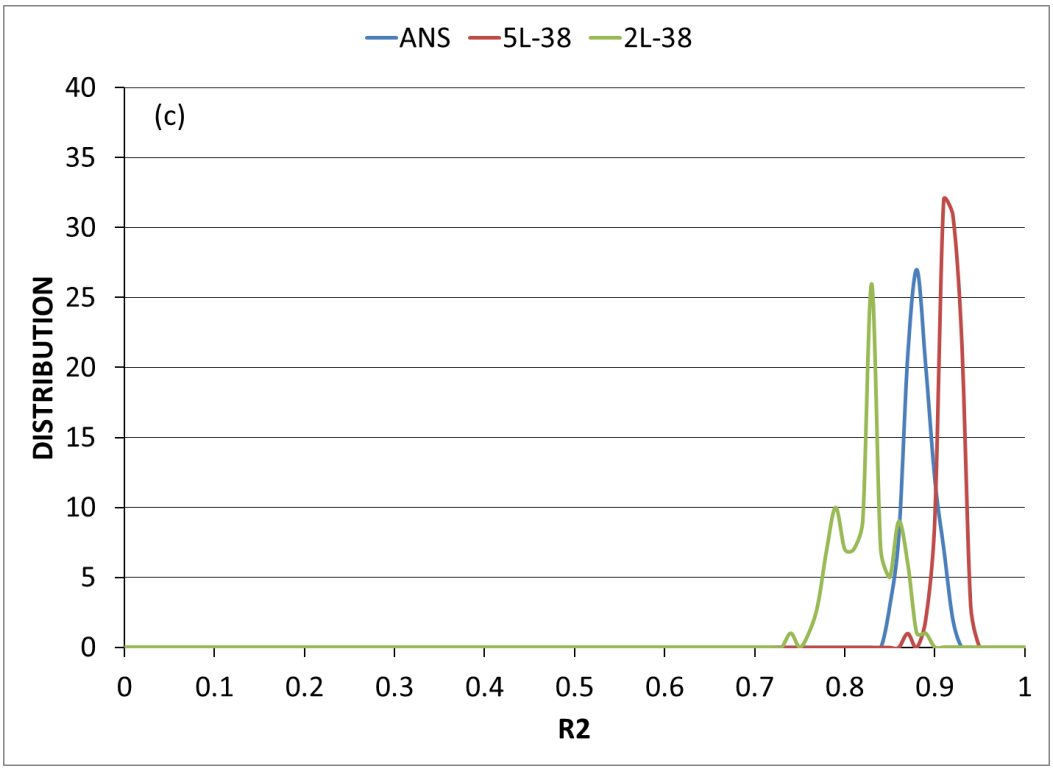

Figure 3: R^2 distributions of ANS-trained models for (a) Vp, (b) Vp ϕ, and (c) Vp ϕ GR WLC

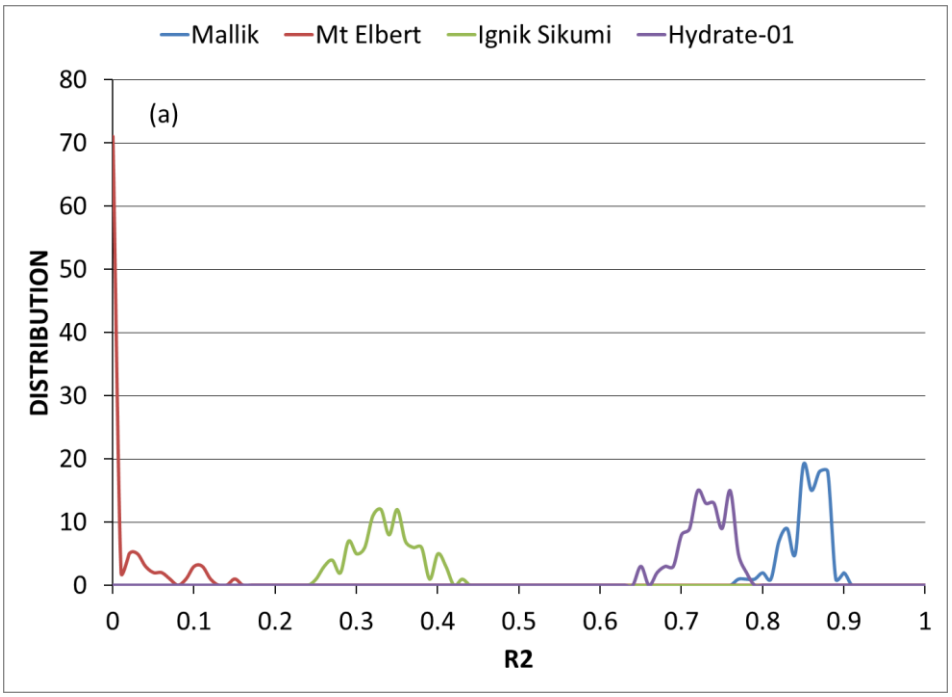

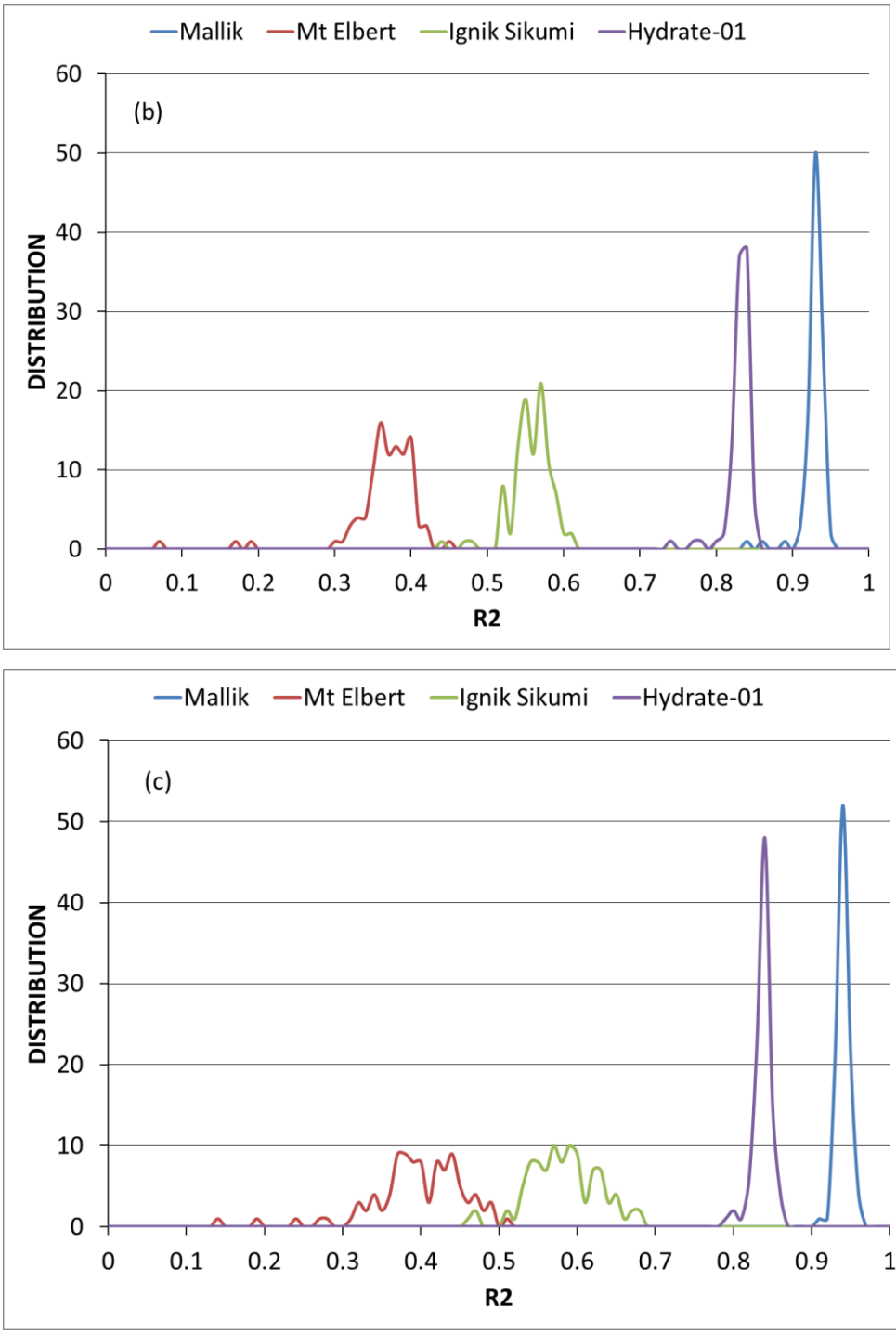

Fig. 4 R^2 distributions of Mallik-trained models for (a) Vp, (b) Vp ϕ, and (c) Vp ϕ GR WLC

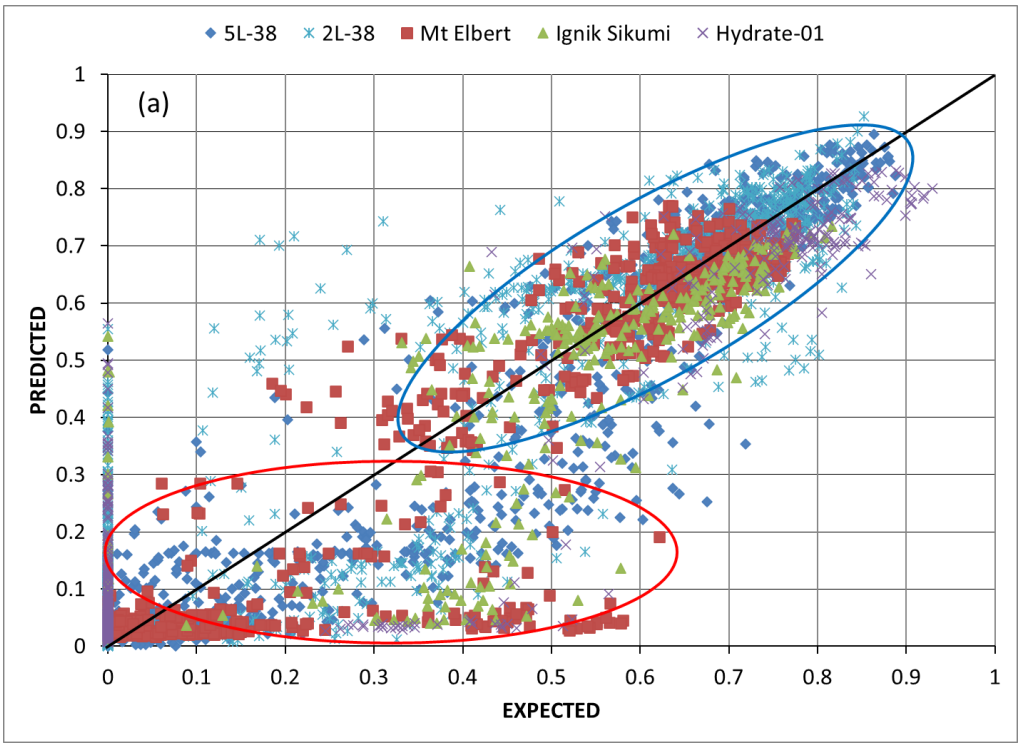

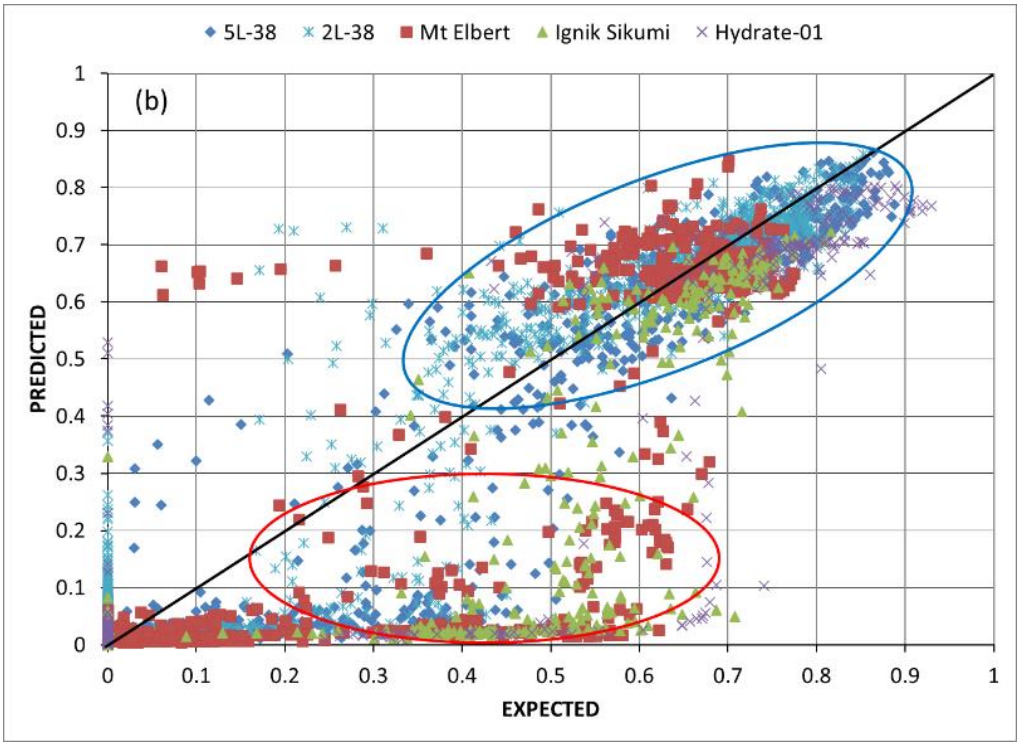

Fig. 5 Prediction vs expectation of a (a) ANS-trained and a (b) Mallik-trained model using Vp ϕ GR WLC

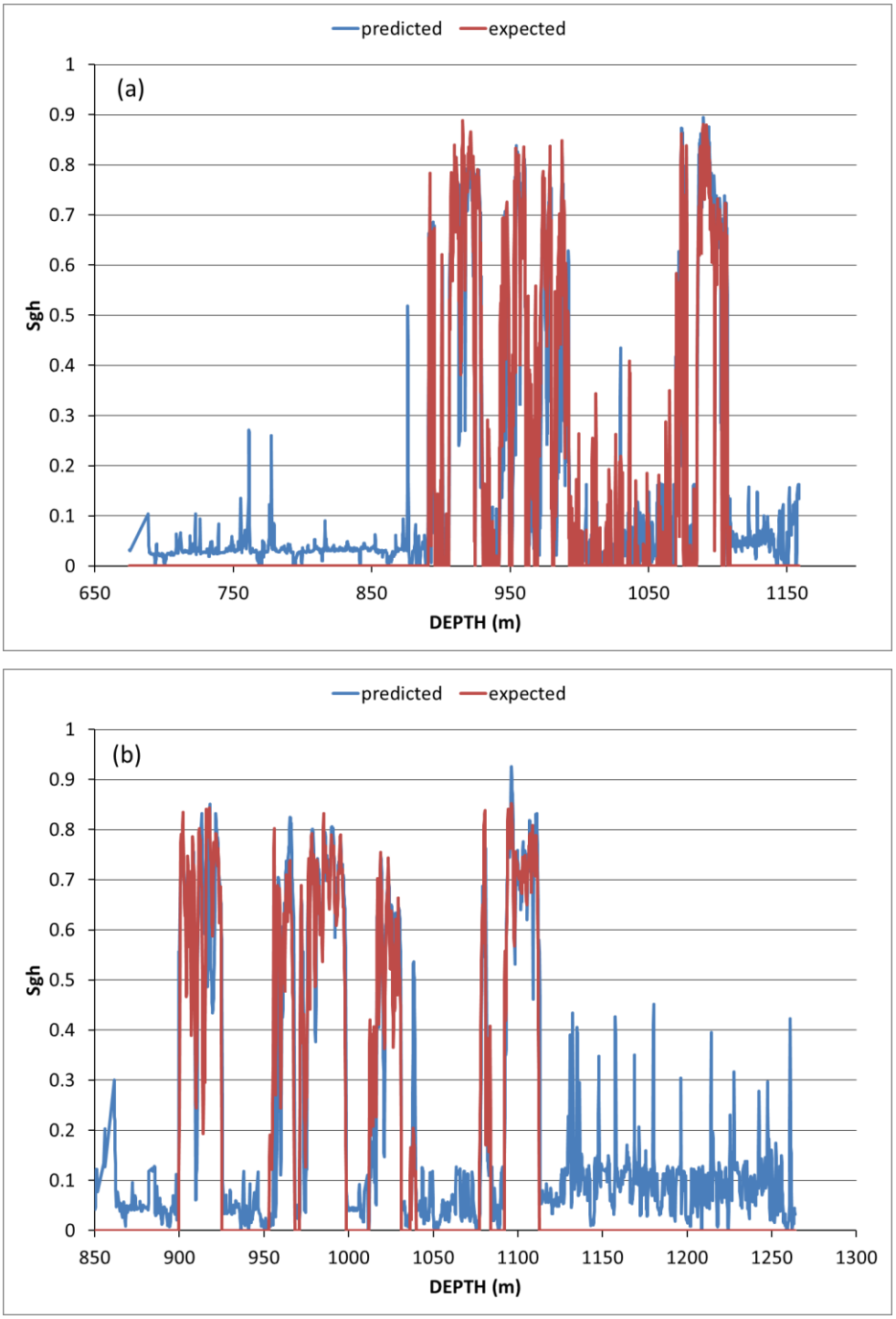

Fig. 6 ANS-trained model predicting gas hydrate saturations using Vp ϕ GR WLC in Mallik wells (a) 5L-38 and (b) 2L-38

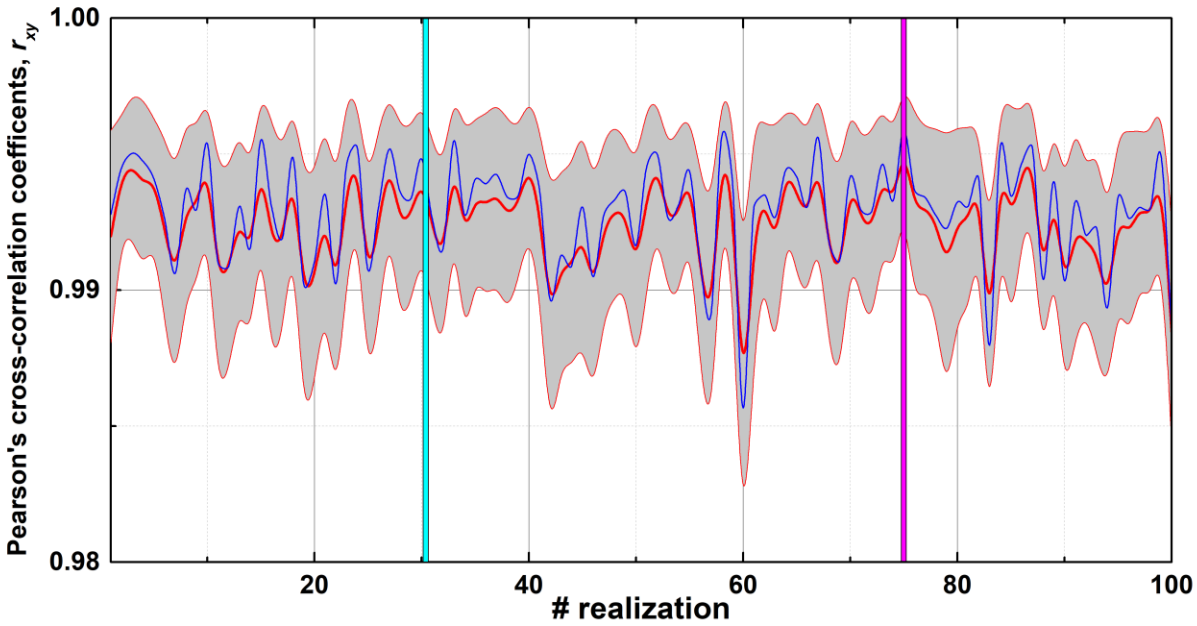

Fig. 7 Averaged Pearson's cross-correlation coefficients for 100 realizations to predict S_{gh} at the Mallik 2L-38 well using the ANS-trained ML model utilizing ϕ *GR Vp* WLC triplets. The gray areas highlight the standard deviation for the coefficient's means (red curves). The median values are shown in blue curves. The cyan and magenta vertical lines designate the realizations corresponding to the averaged R^2 coefficient and the maximum r_{xy}, respectively.

Table 5 Descriptive statistics collected across 100 realizations to predict gas hydrate saturation distributions at the Mallik 2L-38 well using the ANS-trained ML models.

WLC	Score (mean values)	Score (median values)	Pearson's coefficient, r_{xy} at aver. R^2	Averaged R^2	Max Pearson's coefficient, max r_{xy}	R^2 value at max r_{xy}
ϕ, Rt, Vp	99.275	99.335	0.9927	0.9038	0.9950	0.9235
ϕ, GR, Vp	99.245	99.295	0.9923	0.8179	0.9954	0.8267
ϕ, Vp, Vs	98.937	98.983	0.9897	0.5839	0.9932	0.6214

BIBLIOGRAPHY

1. Karpatne, A., Ebert-Uphoff, I., Ravela, S., Babaie, H.A., Kumar, V.: Machine Learning for the Geosciences: Challenges and Opportunities. IEEE Trans. Knowl. Data Eng. 31, 1544–1554 (2019). https://doi.org/10.1109/TKDE.2018.2861006

2. Lary, D.J., Alavi, A.H., Gandomi, A.H., Walker, A.L.: Machine learning in geosciences and remote sensing. Geosci. Front. 7, 3–10 (2016). https://doi.org/10.1016/j.gsf.2015.07.003

3. Caté, A., Perozzi, L., Gloaguen, E., Blouin, M.: Machine learning as a tool for geologists. Lead. Edge. 36, 215–219 (2017). https://doi.org/10.1190/tle36030215.1

4. Karpatne, A., Watkins, W., Read, J., Kumar, V.: Physics-guided Neural Networks (PGNN): An Application in Lake Temperature Modeling. (2017)

5. Racah, E., Beckham, C., Maharaj, T., Kahou, S.E., Prabhat, Pal, C.: ExtremeWeather: A large-scale climate dataset for semi-supervised detection, localization, and understanding of extreme weather events. (2016)

6. Raschka, S., Mirjalili, V.: Python Machine Learning: Machine Learning and Deep Learning with Python, scikit-learn, and TensorFlow 2, 3rd Edition. Packt Publishing (2019)

7. Collett, T., Johnson, A., Knapp, C., Boswell, R.: Natural Gas Hydrates—Energy Resource Potential and Associated Geologic Hazards. American Association of Petroleum Geologists (2009)

8. Dallimore, S.R., Yamamoto, K., Wright, J.F., Bellefleur, G.: Scientific results from the JOGMEC/NRCan/Aurora Mallik 2007-2008 gas hydrate production research well program, Mackenzie Delta, Northwest Territories, Canada. (2012)

9. Anderson, B.J., Kurihara, M., White, M.D., Moridis, G.J., Wilson, S.J., Pooladi-Darvish, M., Gaddipati, M., Masuda, Y., Collett, T.S., Hunter, R.B., Narita, H., Rose, K., Boswell, R.:

Regional long-term production modeling from a single well test, Mount Elbert Gas Hydrate Stratigraphic Test Well, Alaska North Slope. Mar. Pet. Geol. 28, 493–501 (2011). https://doi.org/10.1016/j.marpetgeo.2010.01.015

10. Boswell, R., Schoderbek, D., Collett, T.S., Ohtsuki, S., White, M., Anderson, B.J.: The Iġnik Sikumi Field Experiment, Alaska North Slope: Design, Operations, and Implications for CO 2 –CH 4 Exchange in Gas Hydrate Reservoirs. Energy & Fuels. 31, 140–153 (2017). https://doi.org/10.1021/acs.energyfuels.6b01909

11. Collett, T.S., Zyrianova, M. V, Okinaka, N., Wakatsuki, M., Boswell, R., Marsteller, S., Minge, D., Crumley, S., Itter, D., Hunter, R.D.: Design and operations of the Hydrate 01 Stratigraphic test well, Alaska North Slope, http://pubs.er.usgs.gov/publication/70213245, (2020)

12. Yamamoto, K., Terao, Y., Fujii, T., Ikawa, T., Seki, M., Matsuzawa, M., Kanno, T.: Operational overview of the first offshore production test of methane hydrates in the Eastern Nankai Trough. In: Day 3 Wed, May 07, 2014. OTC (2014)

13. Kumar, P., Collett, T.S., Shukla, K.M., Yadav, U.S., Lall, M.V., Vishwanath, K.: India National Gas Hydrate Program Expedition-02: Operational and technical summary. Mar. Pet. Geol. 108, 3–38 (2019). https://doi.org/10.1016/j.marpetgeo.2018.11.021

14. Boswell, R., Myshakin, E., Moridis, G., Konno, Y., Collett, T.S., Reagan, M., Ajayi, T., Seol, Y.: India National Gas Hydrate Program Expedition 02 summary of scientific results: Numerical simulation of reservoir response to depressurization. Mar. Pet. Geol. 108, 154–166 (2019). https://doi.org/10.1016/j.marpetgeo.2018.09.026

15. Yang, S., Liang, J., Lei, Y., Gong, Y., Xu, H., Wang, H., Lu, J., Holland, M., Schultheiss, P., Wei, J., others: GMGS4 gas hydrate drilling expedition in the South China Sea. Fire ice. 17, 7–11 (2017)

16. Flemings, P., Boswell, R., Collett, T., Cook, A., Divins, D., Frye, M., Guerine, G., Goldberg, D., Malinverno, A., Meazell, K., Morrison, J., Pettigrew, T., Phillips, S., Santra, M., Sawyer, D., Shedd, W., Thomas, C., You, K.: GOM2: Prospecting, Drilling and Sampling Coarse-Grained Hydrate Reservoirs in the Deepwater Gulf of Mexico. (2017)

17. Archie, G.E.: The Electrical Resistivity Log as an Aid in Determining Some Reservoir Characteristics. Trans. AIME. 146, 54–62 (1942). https://doi.org/10.2118/942054-G

18. Lu, S., McMechan, G.A.: Estimation of gas hydrate and free gas saturation, concentration, and distribution from seismic data. GEOPHYSICS. 67, 582–593 (2002). https://doi.org/10.1190/1.1468619

19. Singh, H., Seol, Y., Myshakin, E.M.: Prediction of gas hydrate saturation using machine learning and optimal set of well-logs. Comput. Geosci. 25, 267–283 (2021). https://doi.org/10.1007/s10596-020-10004-3

20. Lee, M.W., Hutchinson, D.R., Collett, T.S., Dillon, W.P.: Seismic velocities for hydrate-bearing sediments using weighted equation. J. Geophys. Res. Solid Earth. 101, 20347–20358 (1996). https://doi.org/10.1029/96JB01886

21. Helgerud, M.B., Dvorkin, J., Nur, A., Sakai, A., Collett, T.: Elastic-wave velocity in marine sediments with gas hydrates: Effective medium modeling. Geophys. Res. Lett. 26, 2021–2024 (1999). https://doi.org/10.1029/1999GL900421

22. Kumar, D., Dash, R., Dewangan, P.: Methods of gas hydrate concentration estimation with field examples. Goehorizons. 76–86 (2009)

23. Collett, T.S., Lee, M.W.: Well Log Characterization of Natural Gas-Hydrates. Petrophysics - SPWLA J. Form. Eval. Reserv. Descr. 53, 348–367 (2012)

24. Jain, V., Saumya, S., Vij, J., Singh, J., Singh, B., Pattnaik, S., Oli, A., Kumar, P., Collett, T.S.:

New technique for accurate porosity estimation from logging-while-drilling nuclear magnetic resonance data, NGHP-02 expedition, offshore, India. Mar. Pet. Geol. 108, 570–580 (2019). https://doi.org/10.1016/j.marpetgeo.2018.11.001

25. Hastie, T., Tibshirani, R., Friedman, J.: The Elements of Statistical Learning: Data Mining, Inference, and Prediction. Springer New York (2013)

26. Breiman, L., Friedman, J.H., Olshen, R.A., Stone, C.J.: Classification And Regression Trees. Routledge (2017)

27. Dudani, S.A.: The Distance-Weighted k-Nearest-Neighbor Rule. IEEE Trans. Syst. Man. Cybern. SMC-6, 325–327 (1976). https://doi.org/10.1109/TSMC.1976.5408784

28. Pal, S.K., Mitra, S.: Multilayer perceptron, fuzzy sets, and classification. IEEE Trans. Neural Networks. 3, 683–697 (1992). https://doi.org/10.1109/72.159058

29. Friedman, J.H.: Multivariate Adaptive Regression Splines. Ann. Stat. 19, (1991). https://doi.org/10.1214/aos/1176347963

30. Hastie, T., Tibshirani, R.: Generalized Additive Models. Stat. Sci. 1, (1986). https://doi.org/10.1214/ss/1177013604

31. Robbins, H., Monro, S.: A Stochastic Approximation Method. Ann. Math. Stat. 22, 400–407 (1951). https://doi.org/10.1214/aoms/1177729586

32. Collett Denver, CO (United States)], T.S. [United S.G.S., Lewis Oklahoma City, OK (United States)], R.E. [Schlumberger W.L.S., Dallimore Pacific Geoscience Centre, Sidney, BC (Canada)], S.R. [Geological S. of C.: JAPEX/JNOC/GSC et al. Mallik 5L-38 gas hydrate production research well downhole well-log and core montages. Natural Resources Canada, Geological Survey of Canada, Vancouver, BC (Canada), Canada (2005)

33. Yang, X.W., Murray, D.R., Noguchi, S., Fujii, T., Fujii, K., Yamamoto, K., Dallimore, S., R:

Geophysical well-log montage for the Aurora/JOGMEC/NRCan Mallik 2L-38 gas hydrate production research well. (2012)

34. Collett, T.S., Lewis, R.E., Winters, W.J., Lee, M.W., Rose, K.K., Boswell, R.M.: Downhole well log and core montages from the Mount Elbert Gas Hydrate Stratigraphic Test Well, Alaska North Slope. Mar. Pet. Geol. 28, 561–577 (2011). https://doi.org/10.1016/j.marpetgeo.2010.03.016

35. Schoderbek, D., Farrell, H., Howard, J., Raterman, K., Silpngarmlert, S., Martin, K., Smith, B., Klein, P.: ConocoPhillips Gas Hydrate Production Test. , Pittsburgh, PA, and Morgantown, WV (United States) (2013)

36. Boswell, R., Collett, T.S., Suzuki, K., Yoneda, J., Haines, S.S., Okinaka, N., Tamaki, M., Crumley, S., Itter, D., Hunter, R.: Alaska North Slope 2018 Hydrate-01 Stratigraphic Test Well: Technical Results. Presented at the (2020)

37. van Stein, B., van Leeuwen, M., Back, T.: Local subspace-based outlier detection using global neighbourhoods. In: 2016 IEEE International Conference on Big Data (Big Data). pp. 1136–1142. IEEE (2016)

38. Ugborugbo, O., Rao, T.: Impact of Borehole Washout on Acoustic Logs and Well-to-Seismic Ties. In: Nigeria Annual International Conference and Exhibition. Society of Petroleum Engineers (2009)

39. Singh, S., Kanli, A.I., Sevgen, S.: A general approach for porosity estimation using artificial neural network method: a case study from Kansas gas field. Stud. Geophys. Geod. 60, 130–140 (2016). https://doi.org/10.1007/s11200-015-0820-2

40. Kleinberg, R.L., Flaum, C., Collett, T.S.: Magnetic resonance log of JAPEX/JNOC/GSC et al. Mallik 5L-38 gas hydrate production research well: gas hydrate saturation, growth habit, and relative permeability. Bull. Surv. Canada. 585, 114 (2005)

41. Haines, S.S., Collett, T., Boswell, R., Lim, T., Okinaka, N., Suzuki, K., Fujimoto, A.: Gas hydrate saturation estimation from acoustic log data in the 2018 Alaska North Slope Hydrate-01 stratigraphic test well. In: Proceedings of the 10th International Conference on Gas Hydrates (ICGH10). US Department of Energy – NETL Program, Singapore (2020)

42. Song, S., Hou, J., Dou, L., Song, Z., Sun, S.: Geologist-level wireline log shape identification with recurrent neural networks. Comput. Geosci. 134, 104313 (2020). https://doi.org/10.1016/j.cageo.2019.104313

43. Kanfar, R., Shaikh, O., Yousefzadeh, M., Mukerji, T.: Real-time well log prediction from drilling data using deep learning. Int. Pet. Technol. Conf. 2020, IPTC 2020. (2020). https://doi.org/10.2523/iptc-19693-ms

44. Baldi, P., Sadowski, P.: The dropout learning algorithm. Artif. Intell. 210, 78–122 (2014). https://doi.org/10.1016/j.artint.2014.02.004

45. Glorot, X., Statistics, Y.B.B.T.-P. of the T.I.C. on A.I. and: Understanding the difficulty of training deep feedforward neural networks, http://proceedings.mlr.press/v9/glorot10a/glorot10a.pdf

46. Saputro, O.D., Maulana, Z.L., Latief, F.D.E.: Porosity Log Prediction Using Artificial Neural Network. J. Phys. Conf. Ser. 739, 012092 (2016). https://doi.org/10.1088/1742-6596/739/1/012092

47. Elsayed, M., Glatz, G., El-Husseiny, A., Alqubalee, A., Adebayo, A., Al-Garadi, K., Mahmoud, M.: The Effect of Clay Content on the Spin–Spin NMR Relaxation Time Measured in Porous Media. ACS Omega. 5, 6545–6555 (2020). https://doi.org/10.1021/acsomega.9b04228

48. Bikmukhametov, T., Jäschke, J.: Combining machine learning and process engineering physics towards enhanced accuracy and explainability of data-driven models. Comput.

Chem. Eng. 138, 106834 (2020). https://doi.org/10.1016/j.compchemeng.2020.106834

49. Arief, H.A., Wiktorski, T., Thomas, P.J.: A Survey on Distributed Fibre Optic Sensor Data Modelling Techniques and Machine Learning Algorithms for Multiphase Fluid Flow Estimation. Sensors. 21, 2801 (2021). https://doi.org/10.3390/s21082801

50. Truc, G., Rahmanian, N., Pishnamazi, M.: Assessment of Cubic Equations of State: Machine Learning for Rich Carbon-Dioxide Systems. Sustainability. 13, 2527 (2021). https://doi.org/10.3390/su13052527

51. Collett, T.S., Lee, M.W., Agena, W.F., Miller, J.J., Lewis, K.A., Zyrianova, M. V., Boswell, R., Inks, T.L.: Permafrost-associated natural gas hydrate occurrences on the Alaska North Slope. Mar. Pet. Geol. 28, 279–294 (2011). https://doi.org/10.1016/j.marpetgeo.2009.12.001

52. Boswell, R., Collett, T.S., Myshakin, E., Ajayi, T., Seol, Y.: The increasingly complex challenge of gas hydrate reservoir simulation. In: Proceedings of the 9th International Conference on Gas Hydrates (ICGH9). , Denver (2017)

53. Yoneda, J., Jin, Y., Muraoka, M., Oshima, M., Suzuki, K., Walker, M., Otsuki, S., Kumagai, K., Collett, T.S., Boswell, R., Okinaka, N.: Multiple physical properties of gas hydrate-bearing sediments recovered from Alaska North Slope 2018 Hydrate-01 Stratigraphic Test Well. Mar. Pet. Geol. 123, 104748 (2021). https://doi.org/10.1016/j.marpetgeo.2020.104748

54. Medioli, B.E., Wilson, N., Dallimore, S.R., Paré, D., Brennan-Alpert, P., Oda, H.: Sedimentology of the cored interval, JAPEX/JNOC/GSC et al. Mallik 5L-38 gas hydrate production well, Mackenzie Delta, Northwest Territories. (2005)